Electronic Supplementary Material (ESI) for Dalton Transactions.

Porous carbonaceous materials simultaneously dispersing N, Fe and Co as bifunctional catalysts for ORR and OER reactions: electrochemical performance in a prototype of Zn-air battery

Daniela Jaramillo[1], German Alvarez[1], Cristian Díaz[1], Sebastián Pérez[2], Juan Muñoz Saldaña[2], Ligia Sierra[1], Betty Lopez[1], Alonso Moreno-Zuria[3], Mohamed Mohamedi[3], Ruben Palacio[1]*

1. Grupo de Investigación Ciencia de los Materiales, Instituto de Química, Facultad de Ciencias Exactas y Naturales, Universidad de Antioquia, Calle 70 No 52 - 21, Medellín, Antioquia, 050010, Colombia.

2. Laboratorio Nacional de Proyección Térmica (CENAPROT), Centro de Investigación y de Estudios Avanzados del IPN, Libramiento Norponiente 2000 Fracc. Real de Juriquilla, 76230 Querétaro, México.

3. Institut National de la Recherche Scientifique (INRS), Énergie Matériaux Télécommunications (EMT), 1650 Boulevard Lionel-Boulet, Varennes, Québec Canada, J3X 1P7, Canada.

Corresponding author: ralberto.palacio@udea.edu.co

1. Porous carbonaceous heterogeneous catalysts preparation

Representation of the preparation of phenanthroline complexes with Fe^{+3} and Co^{+2} and carbonization to obtain N-doped CMK-3 dispersing Fe and Co species.

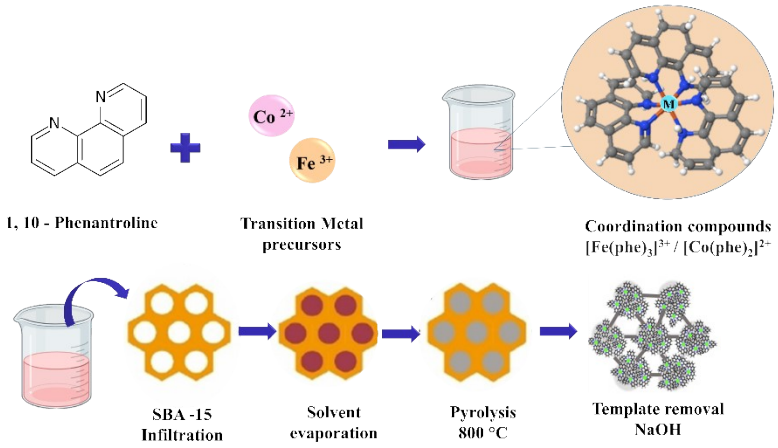

Figure S1. Preparation of N-doped carbonaceous heterogeneous catalysts.

2. Materials characterization

2.1 Complex formation and thermal stability

The infiltrated SBA-15 powder containing Phe (Phe-SBA-15), Fe^{+3}Phe complex (FePhe-SBA-15), Co^{2+}Phe complex (CoPhe-SBA-15), $Fe^{+3}Co^{+2}$Phe complex (FeCoPhe-SBA-15 (1/6)), and $Fe^{+3}Co^{+2}$Phe complex (FeCoPhe-SBA-15 (1/1)) were analyzed by FTIR (Fig. S2a) and TGA (Fig. S2b) in order to study the complex formation and thermal changes during carbonization.

As a first observation, the FTIR spectrum of SBA-15 hard template shows a band centered at 1070 cm^{-1}, characteristic of Si–O–Si vibrations, which is observed after impregnation with Phe or the different Phe-complexes, indicating that any modification of Si-O-Si bonds is induced during the interaction (Fig S2a). After impregnation with Phe (Phe-SBA-15) additional bands can be observed, some of them at 566, 699, 889, 1032, and 1687 cm^{-1}; attributed to Phe, suggesting the filling of the pore system in SBA-15 template. However, after mixing Phe and Fe^{+3} or Co^{+2} ions forming the respective coordination compounds, the characteristic bands of C–N, C=N of Phe are not observed, indicating that interaction of Phe, mainly through N moieties, with metal ions successfully allowed the formation of the complexes while filling the pore system of SBA-15. The presence of the metal ion resulted in a decrease in the intensities as well as a shift of the bands observed for Phe-SBA-15.

Fig. S2b shows the TGA thermogram of pure Phe obtained under N_2-atmosphere. Thermal Phe decomposition initiates at ~150 °C, but the absence of a final residue at higher temperatures indicates that sublimation occurred. In the case of the infiltrated SBA-15 powder with Phe, Phe–SBA-15, two main thermal events are occurring, the first one in the temperature range of ~150-250 °C and the second one in the temperature range of ~250-450 °C, with a final carbonaceous residue of ~40 wt%. This result suggests that the decomposition/carbonization of Phe is modified because of interaction and/or confinement in the pores of SBA-15 hard template, besides the thermal conversion of Phe into a carbonaceous material required higher energy than for free Phe. After filling the pore

structure of SBA-15 with Fe^{+3}Phe complex, FePhe-SBA-15, three main thermal events are observed to take place at lower temperatures than in the case of Phe–SBA-15 composite; this observation suggests that the presence of Fe^{+3} ions influenced the thermal conversion of Phe, perhaps catalyzing its thermal decomposition. In the case of CoPhe-SBA-15, three main thermal events are observed, and the thermal conversion of CoPhe-SBA-15 demands higher temperatures than in the case of the FePh-SBA-15. This result indicates a stronger interaction between Co^{+2} and Phe than between Fe^{+3} and Phe. Phe has pyridinic N moieties, according to Pearson's Hard Soft Acid Base (HSAB) principles, pyridine is a borderline base [1], whereas Fe^{+3} ions are hard acids and Co^{+2} ions are boundary acids. In agreement with HSAB principles, hard acids interact strongly with hard bases and soft acids interactions are stronger with soft bases. For instance, interactions between Co^{+2} and Phe are stronger than between Fe^{+3} and Phe. As a result, Co–Phe decomposes at higher temperatures. Finally, when using a mixture of both, Fe^{+3} and Co^{+2} with Phe, slightly higher temperatures are required for the thermal conversion of the complexes into carbonaceous materials containing metal ions, resulting in a fourth thermal event at temperatures above 650 °C.

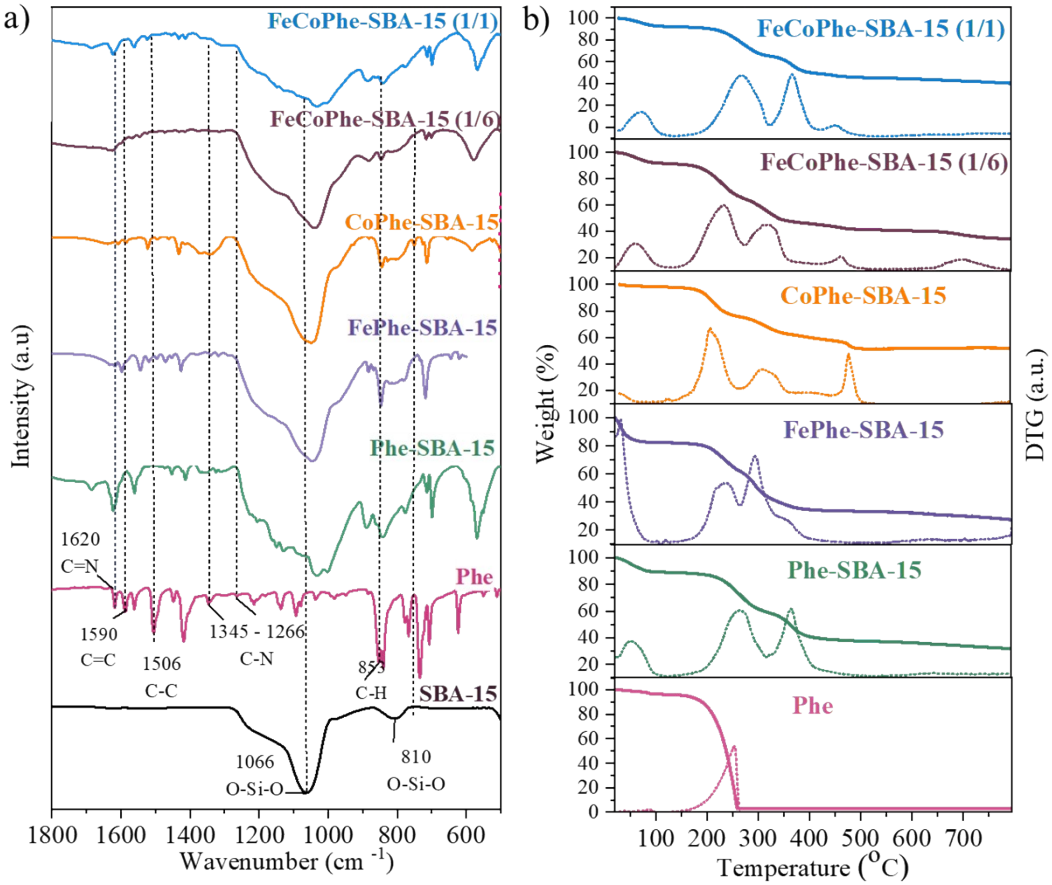

Figure S2. Characterization of metal complex infiltrated SBA-15 template using a) FTIR and b) TGA-DTG under N_2 atmosphere.

2.2 Raman spectroscopy characterization

Carbonaceous materials typically exhibit two characteristic bands, associated with vibrational modes of first-order, between 1100 - 1700 cm^{-1}, referred to as D-band, which is associated with the presence of amorphous carbon structures, grain boundaries/defects in the lattice structure; and the G band is associated to sp^2-bonded C-C in carbon materials indicating an ordered carbon structure and/or a graphitic character of the structure [2].

To compare different carbonaceous materials, the ratio I_D/I_G or A_D/A_G is generally used to describe differences in purity and/or the quality of the carbonaceous materials in terms of graphitic degree. All spectra present the two characteristic bands, the D band centered between 1323-1338 cm^{-1}, and the G band centered between 1565-1575 cm^{-1} (Fig. S3). Spectrum deconvolution by Gaussian functions suggests that the D band has two or three contributions: D1 or D band centered at 1350 cm^{-1} related to the graphene-like layer edges with an A_{1g} symmetry, D4 band centered at 1200 cm^{-1} related to the presence of polyenes and ionic impurities, while the D2 or D' is adjacent to the G peak and is related to defects in the graphene-like layers with a E_{2g} symmetry [2].

For all samples, the intensity and area of the G band were lower than for those of the D1 band, indicating a low degree of graphitization which can be attributed to the relatively low temperature of carbonization. This result also demonstrates a higher degree of defects in the carbonaceous materials, the ratio A_D/A_G (where A_D is the sum of the areas of all contributions of D bands) is higher than 2.5 (Fig. S3), which is in agreement with the objective of the present work *i.e.,* creating defects on the carbonaceous materials as potential active sites for ORR and OER reactions.

On the other hand, the Raman spectrum of CoNCMK-3 shows three Raman peaks of low intensity and poor resolution at 456, 508, and 659 cm^{-1}, which match with the vibrational modes of Co_3O_4 in the spinel structure: E_g, F_{2g} and A_{1g}, respectively [3]. This result indicates that part of Co could be dispersed in the carbonaceous lattice and another part is forming Co spinel particles, but in the case of Co containing bimetallic samples, FeCoNCMK-3 (1/6) and FeCoNCMK-3 (1/1), no Raman peaks are observed for Co_3O_4 spinel.

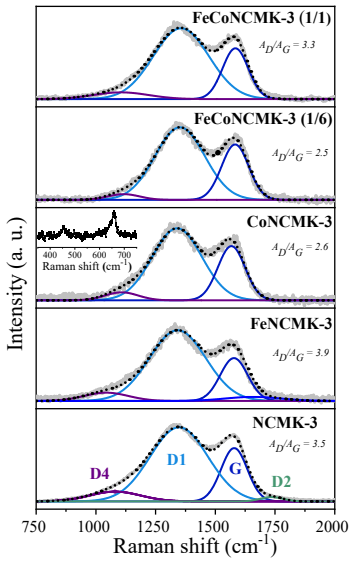

Figure S3. Raman spectra and A_D/A_G ratio for: NCMK-3, FeNCMK-3, CoNCMK-3, FeCoNCMK-3 (1/6), FeCoNCMK-3 (1/1) materials.

2.3 HRTEM characterization of sample FeCoNCMK-3 (1/1)

HRTEM analysis was performed on a FeCoNCMK-3 (1/1) powder without being sliced in the microtome (Fig. S4). The micrographs show grains with well-defined, rope-like morphology and porosity, forming elongated aggregates as previously observed by SEM (Fig. 3). EDX analysis (Fig. S4b and S4c) revealed the presence of Fe, Co, and N in the observed grains, suggesting a high dispersion of these elements in the carbonaceous materials. These results at the nanometric scale agree with SEM-EDS analysis at micrometric scale, evidencing that Fe and Co are present in the same areas of the NCMK-3, showing an even distribution of both metals. Particles of Fe, Co, or FeCo are not observed neither inside the mesopores in the grains of NCMK-3 support nor on the outer surface of the grains, suggesting a high dispersion of iron and cobalt species at the atomic level.

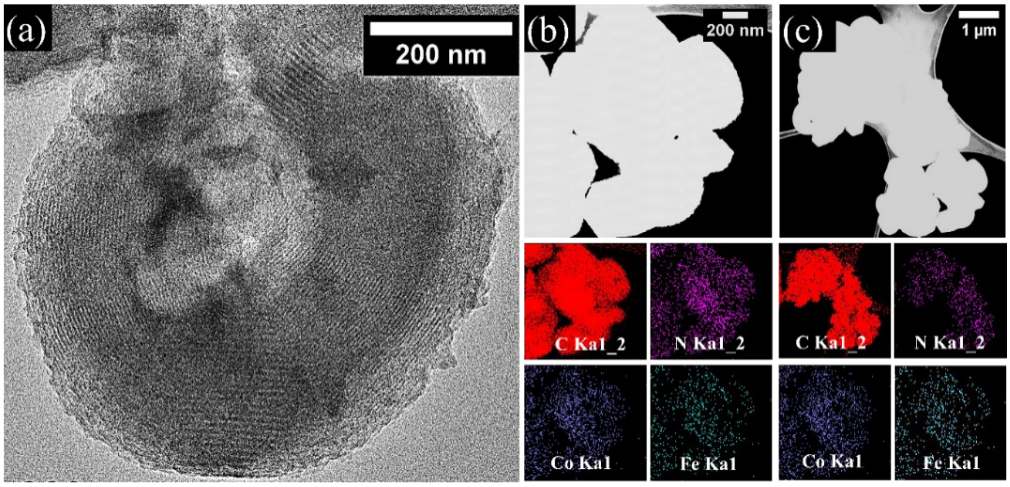

Figure S4. HRTEM analysis for FeCoNCMK-3 (1/1) sample: a) TEM micrograph for powder without being sliced, b-c) HRTEM mapping analysis.

2.4 XPS characterization

Signal Processing:

The values of the Relative Sensitivity Factors (RSF), obtained from the Scofield database were C 1s (1.0000), N 1s (1.6002), O 1s (2.2572), Fe 2p (10.2155), and Co 2p (10.7132). The XPS spectra were analyzed using CasaXPS software, all signals were treated using an Off Shirley background, asymmetric functions using a line shape SGL(p)T(k), and restrictions were imposed as indicated below:

- Signals 1s: all the peaks have the same FWHM.
- Signals 2p, with spin-orbit coupling $2p_{3/2}$ and $2p_{1/2}$: all the peaks for $2p_{3/2}$ have the same FWHM and all the peaks for $2p_{1/2}$ have the same FWHM. The satellite structure in the case of Co 2p and Fe 2p signals was complex and with low resolution. Restrictions were also imposed to the area ratio of signal $2p_{1/2}$ with respect to the signal $2p_{3/2}$, the area of peaks associated with signals $2p_{1/2}$ being 0.5 of that of peaks associated with $2p_{3/2}$ signals.

Results of C 1s and O 1s:

The high-resolution C 1s spectrum for metal-free NCMK-3 (Fig. S4) shows 6 different C species with binding energies of 284.8 eV and 285.8 eV for C–C (C sp^3)/C=C (C sp^2), C–O(H)/C–N bonds in pyridinic-N and pyrrolic–N; 286.5 eV for C–O bonds in esters and lactones/C–N in graphitic-N/C–N=O bonds in nitrogen oxides; 287.6 eV for N–C(O)–C/C=O bonds; 289 eV for O–C=O/N–(CO)–N/N–(CN)–N bonds; and 290.4 eV. The last signal, in particular, is difficult to correlate with a specific C species. It may be attributed to π-π* satellite peak or to be associated with a more complex chemical environment with C atoms losing electronic density, similar to O–C=O/O=C–N as C atoms simultaneously bonded to O and N will be electronically deficient [4-6].

The high-resolution C 1s spectrum for metal-containing materials can be convoluted into 5 components for monometallic samples and 6 components for bimetallic samples (Fig. S5). This result indicates that the presence of metal/metal ions modifies the speciation of C on the surface and/or that because of the complex chemical interactions between C, N, O, and metals it is more difficult to readily identify all the species on the surface. The spectra show signals at 284.6±0.2 eV for C–C (C sp^3)/C=C (C sp^2), C–O(H)/C–N bonds in pyridinic-N and pyrrolic-N species, the signal at 285.5±0.2 eV for C–N bonds; at 286.5±0.2 eV for C–O bonds in esters and lactones/C–N in graphitic-N/C–N=O bonds in nitrogen oxides; at 287.6±0.3 eV for N–C(O)–C/C=O bonds, 288.8±0.3 eV for O–C=O/N–(CO)–N/N–(CN)–N bonds. The spectra of monometallic samples, CoNCMK-3 and FeNCMK-3, do not show the signal at 290 eV compared with metal-free NCMK-3, attributed to π–π* satellite peak, this could indicate a less graphitic and/or electron deficient surface.

The high-resolution O 1s spectrum (Fig. S5) for metal-free and samples containing iron shows different O species with binding energies of 530.7±0.3 eV for C=O (quinone); 532.3±0.2 eV for C–O/O=C–O bonds; 533.5±0.2 eV for chemisorbed N=O/COOH and/or adsorbed H_2O [7, 8]. Finally, the spectra show a peak centered at 535.7 eV.

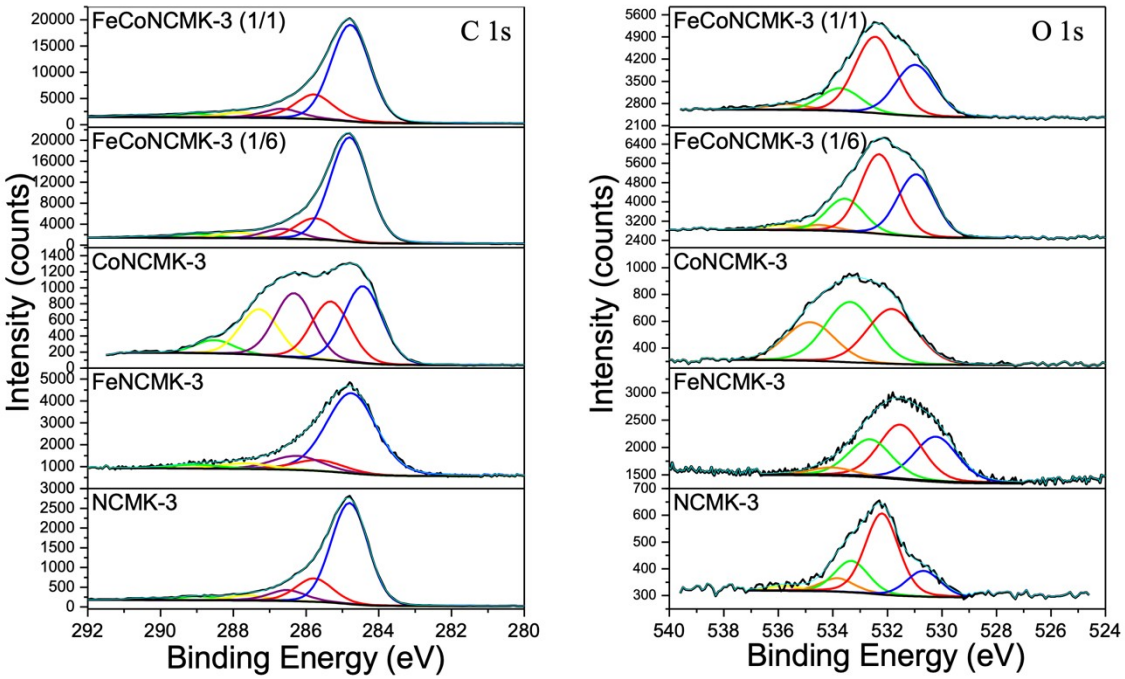

Figure S5. High resolution XPS characterization of materials for C 1s and O 1s species.

3. Stability tests: chronoamperometric measurements

The stability of the Ag/AgCl reference electrode was evaluated using ciclyc voltammetry, 100 cycles, between 0.2 and 2.0 V vs RHE at 20 mV s^{-1} in N_2-atmosphere (Fig. S6a) and O_2-atmosphere (Fig. S6b). Comparing the cycles 1, 10, 50, and 100 there is no change in the voltagrams in any of the atmospheres evaluated, indicating that the Ag/AgCl reference electrode is stable under operating conditions for moderately long times of analysis.

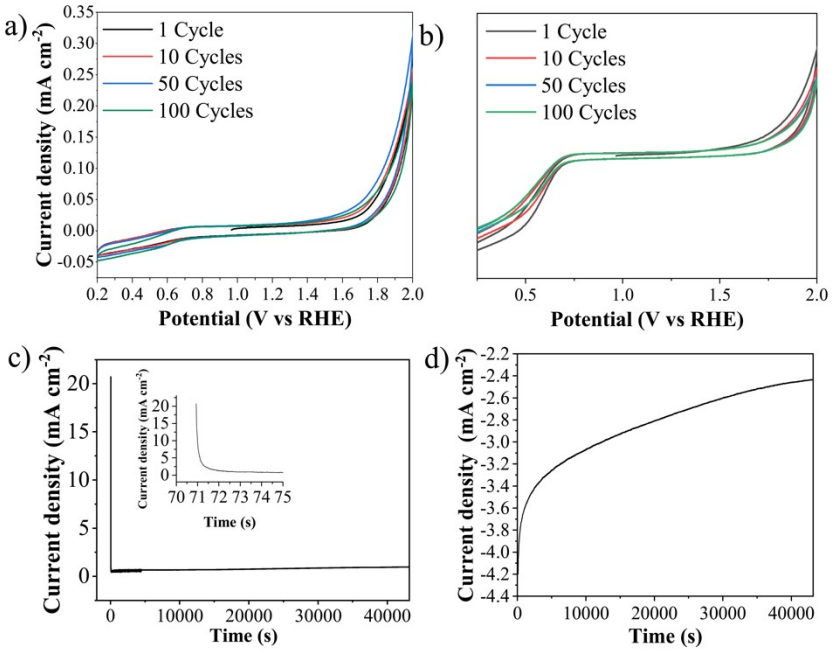

Figure S6. Cyclic voltammetry for Ag/AgCl electrode without any catalyst, between 0.2 and 2.0 V vs RHE on a) N_2-atmosphere, b) O_2-atmosphere. Chronoamperometric results for FeCoNCMK-3 (1/1) for 12 h at c) 1.68 V vs RHE, for OER and d) 0.54 V vs RHE, for ORR.

4. O_2 production during OER:

As a first remark, it is necessary to consider that the evaluation of the electrocatalytic activity in OER reaction is performed under a continuous flow of N_2, 100 mL min^{-1}. For instance, the produced O_2 is evacuated at a high flow rate, thus the detection and O_2 concentration per unit of time are difficult to quantify, and analytical limitations are thus restrictive for the measure. It is also necessary to consider the low amount of heterogeneous catalyst used in the cathode electrode in a reactor with a volume of 100 mL filled with 60 mL of solution. The results are within the limits of the detection of the instrument.

As a second remark, reported data for OER reaction, O_2 evolution, with a carbon reference GC and with the carbonaceous support without metals are also provided in the manuscript.

The data, obtained during the chronoamperometric evaluation, considering as reference a bituminous coal, showed that:

- CO_2 is not detected under the reaction's conditions.

- O_2 is detected with a concentration in the gas outlet flow between 0.1 and 1.3 vol.%

Table S1. Quantity of O_2 generated at various reaction times at 0.6 V vs RHE for FeCoNCMK-3 (1/1) catalyst.

Reaction time (s)	Concentration: O_2 vol% generated
0	0
300	0.1
1600	1.3
2000	1.3
3000	1.3
3400	1.3
3600	1.3

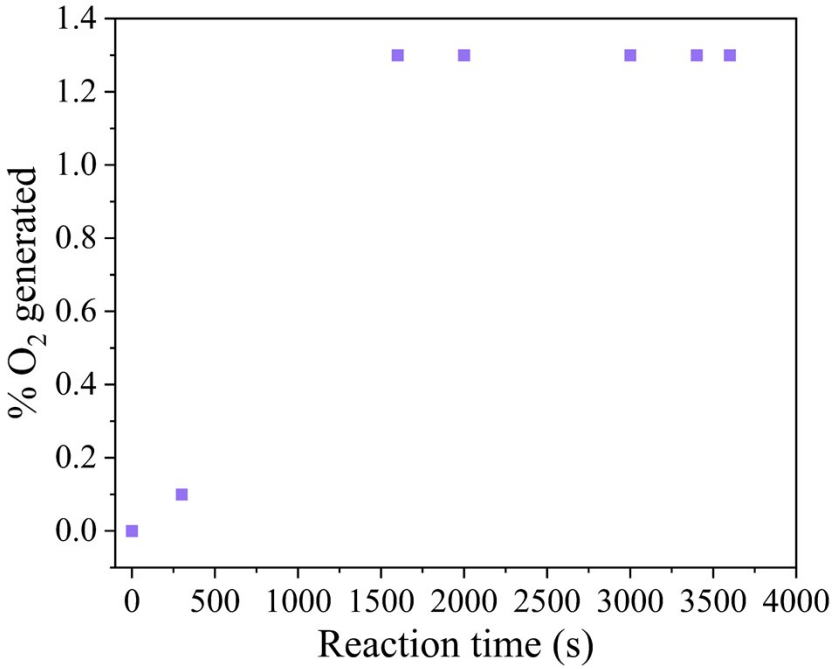

Figure S7. Schematic representation of the O_2 generated at various reaction times at 0.6 V vs RHE for FeCoNCMK-3 (1/1) catalyst.

5. References

1. Pearson, R. G., Hard and soft acids and bases, HSAB, part 1: Fundamental principles. *J. Chem. Educ.* **1968,** *45* (9), 581.

2. Thapliyal, V.; Alabdulkarim, M. E.; Whelan, D. R.; Mainali, B.; Maxwell, J. L., A concise review of the Raman spectra of carbon allotropes. *Diamond Relat. Mater.* **2022,** *127*, 109180.

3. Hadjiev, V. G.; Iliev, M. N.; Vergilov, I. V., The Raman spectra of Co 3 O 4. *Journal of Physics C: Solid State Physics* **1988,** *21* (7), L199.

4. Ayiania, M.; Smith, M.; Hensley, A. J. R.; Scudiero, L.; McEwen, J.-S.; Garcia-Perez, M., Deconvoluting the XPS spectra for nitrogen-doped chars: An analysis from first principles. *Carbon* **2020,** *162*, 528-544.

5. Ding, Y.; Tang, Y.; Yang, L.; Zeng, Y.; Yuan, J.; Liu, T.; Zhang, S.; Liu, C.; Luo, S., Porous nitrogen-rich carbon materials from carbon self-repairing g-C3N4 assembled with graphene for high-performance supercapacitor. *Journal of Materials Chemistry A* **2016,** *4* (37), 14307-14315.

6. Chiang, C. L.; Yang, J. M., Flame retardance and thermal stability of polymer/graphene nanosheet oxide composites. In *Novel Fire Retardant Polymers and Composite Materials*, 2017; pp 295-312.

7. Chen, J.; Xu, J.; Zhou, S.; Zhao, N.; Wong, C.-P., Nitrogen-doped hierarchically porous carbon foam: A free-standing electrode and mechanical support for high-performance supercapacitors. *Nano Energy* **2016,** *25*, 193-202.

8. Xu, B.; Zheng, D.; Jia, M.; Cao, G.; Yang, Y., Nitrogen-doped porous carbon simply prepared by pyrolyzing a nitrogen-containing organic salt for supercapacitors. *Electrochim. Acta* **2013,** *98*, 176-182.